PAPER Nr.: 23

IRROTATIONAL AND ROTATIONAL TRANSONIC FLOWS USING A BOUNDARY INTEGRAL EQUATION METHOD

by

M. Gennaretti, U. Iemma, F. Salvatore, L. Morino
Terza Università di Roma, Dipartimento di Meccanica e Automatica, Rome, Italy

TWENTIETH EUROPEAN ROTORCRAFT FORUM
OCTOBER 4 - 7, 1994 AMSTERDAM

Printed by the Technical Highschool Haarlem

IRROTATIONAL AND ROTATIONAL TRANSONIC FLOWS USING A BOUNDARY INTEGRAL EQUATION METHOD

M. Gennaretti, U. Iemma, F. Salvatore and L. Morino

Terza Università, Dipartimento di Meccanica e Automatica, Rome, Italy

1. INTRODUCTION

This paper deals with some recent developments of a boundary integral equations methodology for the analysis of irrotational and rotational transonic flows. The presence of vorticity, in the transonic regime, is caused both by viscous effects inside the boundary layer and by the curvature of the shock. Commonly, viscous effects are taken into account in the interactive boundary layer techniques, whereas the shock curvature vorticity is the main issue in Euler method analyses (for a review on the subject, see [1] and [2]). Whenever the transonic flow is such that the shock generated is weak, then the vorticity beyond the discontinuity is negligible and the interactive boundary layer methodology can satisfactorily predict the dynamics of the flow. This is the case that we intend to analyze in this work.

Here, the effects of the rotationality in the field are evaluated by using a potential-vorticity decomposition introduced in [3] which. As shown in [4] and [5], for negligible shock-induced vorticity and for high Reynolds number flows, this decomposition reduces to the well-known transpiration velocity approach introduced by Lighthill [6]. This implies a source-sink distribution over the body and wake surfaces in order to take into account the influence of the rotationality of the flow on the external solution.

For the irrotational term in the decomposition, the aerodynamic analysis is performed by using a boundary integral formulation for the conservative full-potential form of the wave equation for the velocity potential, introduced by Morino and Iemma [7] and applied to helicopter rotors in hover in [8]. In the numerical implementation only the region of the flow close to the body (where the non-linear effects are important) has to be included in the computation. The method is shock-capturing and artificial dissipation is introduced in the supersonic region of the field by a flux-upwinding technique.

The boundary-layer flow is here analyzed by an integral approach. The laminar region is studied by a modification of the simple, but realistic, Thwaites' formula [9], whereas the turbulent-flow evolution is described by the lag-entrainment method, introduced by Green, Weeks and Brooman [10].

The boundary-element full-potential formulation has already been validated for steady, three-dimensional flows. Some results for fixed wings [11] and recently obtained results for hovering rotors in the transonic regime are presented here. The formulation for viscous flows is presented for the general case. The validation is limited to steady two-dimensional attached flows; as mentioned above, in this

case the formulation reduces to that by Lighthill [6] (transpiration velocity approach). Specifically, two-dimensional subsonic viscous flow configurations are considered first in order to test the interactive technique introduced here. Finally, results for viscous transonic flows around airfoils are obtained by matching the full-potential formulation with the above mentioned technique for the analysis of the viscous effects.

2. BOUNDARY INTEGRAL FORMULATION FOR EXTERNAL FLOW

Here, we give an outline of the boundary integral formulation for potential transonic flows. For the sake of simplicity, we limit ourselves to fixed wing analysis (the formulation for rotary wings described extensively in Iemma, Gennaretti and Morino [8] is very closely related to that for fixed wings).

The differential equation governing the motion of an isentropic irrotational flow is the full-potential equation, which is written here in the form of a non-linear wave equation. In a frame of reference rigidly connected with the body translating with velocity $\mathbf{v}_B = -U_\infty \mathbf{i}$, we have

$$\nabla^2\phi - \frac{1}{a_\infty^2}\frac{d_B^2\phi}{dt^2} = \sigma \tag{1}$$

where σ represents all the non-linear terms, whereas $d_B/dt = \partial/\partial t + U_\infty \partial/\partial x$ is the time derivative following a point in a frame of reference fixed with the undisturbed flow. Equation 1 is derived by combining the conservative form of the continuity equation with Bernoulli's theorem for isentropic potential compressible flow, and by taking into account the isentropic density-enthalpy relation. The expression for σ is

$$\sigma = \nabla \cdot \mathbf{b} - \frac{\partial \hat{b}}{\partial t} \tag{2}$$

where

$$\mathbf{b} = \left(1 - \frac{\rho}{\rho_\infty}\right)\nabla\phi - \hat{b}\, U_\infty \mathbf{i}, \qquad \hat{b} = \frac{\rho}{\rho_\infty} + \frac{1}{a_\infty^2}\frac{d_B\phi}{dt} \tag{3}$$

whereas ρ/ρ_∞ is obtained from the Bernoulli theorem as $\rho/\rho_\infty = \left[1 - \left(\dot{\phi} + v^2/2\right)/h_\infty\right]^{1/\gamma-1}$.

The boundary conditions complete the differential problem. These are the impermeability of the body surface $\mathcal{S}_B$, or $\partial\phi/\partial n = \mathbf{v}_B \cdot \mathbf{n}$ for $\mathbf{x}$ on $\mathcal{S}_B$, and $\phi = 0$ at infinity. In addition, we have the conditions on the wake surface $\mathcal{S}_W$, *i.e.*, continuity of pressure, $\Delta p = 0$, and no penetration, $(\mathbf{v} - \mathbf{v}_W) \cdot \mathbf{n}$, where $\mathbf{v}_W$ is the velocity of a point of the wake. These yield (i) $\Delta\left(\partial\phi/\partial n\right) = 0$, and (ii) $D_W(\Delta\phi)/Dt = 0$ for $\mathbf{x}$ on $\mathcal{S}_W$ (where $D_W/Dt = \partial/\partial t + \mathbf{v}_W \cdot \nabla$, with $\mathbf{v}_W = (\mathbf{v}_1 + \mathbf{v}_2)/2$, where $\mathbf{v}_1$ and $\mathbf{v}_2$ denote the velocity on the two sides of the wake); condition (ii) implies that $\Delta\phi$ is constant following a wake point $\mathbf{x}_W$, mantaining the same value it had when $\mathbf{x}_W$ was leaving the trailing edge (see Morino [12] for details).

Next, for the sake of clarity, we limit our presentation to the steady-state case (although in the actual computation the steady solution is obtaibed through a time marching technique, described in [8] and [13]). Then, applying the classical Prandtl-Glauert transformation of coordinates

$$x_0 = x/\beta; \quad y_0 = y; \quad z_0 = z \tag{4}$$

where $\beta = (1 - M_\infty^2)^{1/2}$, with $M_\infty = U_\infty / a_\infty$, Eq. 1 reduces to the Poisson equation

$$\nabla_0^2 \phi = \sigma_0 \tag{5}$$

where ∇_0^2 is the Laplacian operator in the Prandtl-Glauert space, and

$$\sigma_0 = \frac{1}{\beta} \frac{\partial b_x}{\partial x_0} + \frac{\partial b_y}{\partial y_0} + \frac{\partial b_z}{\partial z_0} \tag{6}$$

is the resulting expression for the non linear terms.

Next, using the second Green formula applied to a volume outside a surface which surrounds body and wake and recalling that $\Delta(\partial\phi/\partial n) = 0$, one obtains in the limit the following integral representation for the velocity potential in the Prandtl-Glauert space

$$\phi(\mathbf{x}_{0_*}) = \oiint_{\mathcal{S}_B} \left(G \frac{\partial \phi}{\partial n_0} - \phi \frac{\partial G}{\partial n_0} \right) d\mathcal{S} - \iint_{\mathcal{S}_W} \Delta\phi \frac{\partial G}{\partial n_0} \, d\mathcal{S} + \iiint_{\mathcal{V}} \sigma_0 \, G \, d\mathcal{V} \tag{7}$$

where the unit source $G = -1/4\pi \|\mathbf{x}_0 - \mathbf{x}_{0_*}\|$ satisfies the equation $\nabla_0^2 G = \delta(\mathbf{x}_0 - \mathbf{x}_{0_*})$, whereas $\mathcal{S}_B$ is the body surface, $\mathcal{S}_W$ is the wake surface, and $\mathcal{V}$ denotes the fluid region outside the body.

If $\sigma_0 = 0$ (linear case) and $\mathbf{x}_{0_*} \in \mathcal{V}$, Eq. 7 is an integral representation of $\phi(\mathbf{x}_{0_*})$, as a function of ϕ and $\partial\phi/\partial n_0$ on $\mathcal{S}_B$ and of $\Delta\phi$ on $\mathcal{S}_W$. On the other hand, if $\mathbf{x}_{0_*}$ is on $\mathcal{S}_B$, Eq. 7 represents a compatibility condition between ϕ and $\partial\phi/\partial n_0$ on $\mathcal{S}_B$ and $\Delta\phi$ on $\mathcal{S}_W$ for any function ϕ satisfying Eq. 7. Since $\partial\phi/\partial n$ is known from the boundary conditions, and $\Delta\phi$ is constant along a wake streamline and equal to the value at the trailing edge, then Eq. 7 corresponds to a boundary integral equation for ϕ. In the nonlinear case ($\sigma_0 \neq 0$) the integral equation is solved by iterations. Two different approaches are introduced for the numerical evaluation of the volume integral of Eq. 7. In the first one, an integration by parts of the non-linear integral term is introduced in order to avoid the evaluation of the divergence operator, whereas in the second approach the volume integral is discretized in its original form (see [8] and [13] for further details).

3. VORTICITY INFLUENCE ON POTENTIAL FLOW

Next, in order to take into account the effects of vorticity on the potential flow, we discuss some results obtained from a potential-vorticity decomposition introduced by Morino [3]. These results concern some theoretical developments which provide an integral representation for the potential in the exterior region (that outside the vortical region), based on the knowledge of the vorticity distribution. Therefore, it may be applied also for viscous transonic flows, where vorticity is generated both on the body wall and on the shock surface. For high-Reynolds-number flows in presence of weak shocks the resulting interaction formula reduces to the well-known Lighthill transpiration velocity method (see [4] and [5] for details). Here, for the sake of clarity, only the incompressible 2-D flow case will be presented.

Consider the following decomposition for the velocity field, as seen in a frame of reference fixed with the body

$$\mathbf{v} = \nabla\varphi + \mathbf{w} + \mathbf{v}_\infty \tag{8}$$

with $\nabla \times \mathbf{w} = \omega \, \mathbf{k}$, *i.e.*,

$$\frac{\partial w_y}{\partial x} - \frac{\partial w_x}{\partial y} = \omega \tag{9}$$

A particular solution of Eq. 9 is given by

$$\begin{aligned} w_x(x,y) &= 0 \\ w_y(x,y) &= \int_0^x \omega \, dx' \end{aligned} \tag{10}$$

where $w_x = 0$ is an arbitrary, but legitimate assumption.

Next, applying the divergence operator on Eq. 8 one obtains the Poisson equation for the potential

$$\nabla^2 \varphi = -\nabla \cdot \mathbf{w} \tag{11}$$

which, following the same procedure used to obtain Eq. 7, yields the following integral representation

$$\varphi(\mathbf{x}_*) = \oint_{S_B} \left(\chi G - \varphi \frac{\partial G}{\partial y} \right) dx + \iint_{\mathcal{A}_F} \mathbf{w} \cdot \nabla G \, d\mathcal{A} \tag{12}$$

where $\mathcal{A}_F$ denotes the fluid field outside the body, whereas $\chi = -\mathbf{v}_\infty \cdot \mathbf{n}$, with $\mathbf{n}$ denoting the unit vector normal to the body wall. To complete the method, the transport vorticity equation is needed in order to determine $\mathbf{w}$, and hence the field term in the integral representation Eq. 12.

However, as shown in [4] and [5], Eq. 12 may be recast into a novel format in order to obtain a convenient expression for the external potential ϕ. To this aim, we introduce the integral quantities

$$\omega_0(x,y) = \int_y^\infty \omega \, dy'; \quad \omega_1(x,y) = \int_y^\infty \omega_0 \, dy' \tag{13}$$

Assuming the following expression for the vorticity (valid for thin attached boundary layer flows)

$$\omega(x,y) = -\frac{\partial u}{\partial y} \tag{14}$$

for $\mathbf{v} = u\,\mathbf{i} + v\,\mathbf{j}$, Eqs. 13 become

$$\omega_0(x,y) = u - u_e; \quad \omega_1(x,y) = \int_y^\delta (u - u_e) \, dy' \tag{15}$$

where δ is the boundary-layer thickness, whereas u_e is the flow velocity at the outer edge of the boundary layer. Combining Eq. 12 with Eqs. 10 and 15, after lenghty manipulations, one obtains [4, 5]

$$\begin{aligned} \varphi_e(\mathbf{x}_*) &= \oint_{S_B} \left[(\chi + v_{tr}) G - \varphi_e \frac{\partial G}{\partial y} \right] dx + \int_{S_W} \left(v_{tr} G - \Delta\varphi_e \frac{\partial G}{\partial y} \right) dx \\ &+ \iint_{\mathcal{A}_F} \left[\left(\frac{\partial}{\partial x} \int_y^{\delta(x)} (u_e - u) \, dy' \right) + v \right] \frac{\partial G}{\partial y} \, d\mathcal{A} \end{aligned} \tag{16}$$

where $\varphi_e = \phi$ outside the vortical region, whereas v_{tr} is the transpiration velocity introduced by Lighthill [6], given by $v_{tr} = \partial(u_e \, \delta^*)/\partial x$. Therefore, the resulting expression for the external potential contains the desired vorticity-influence terms: (i) a source-sink distribution over the body and wake as already indicated by Lighthill [6], and (ii) a doublet distribution in the rotational field which allows Eq. 16 to be applied also for some of those cases where the Lighthill correction is no more satisfactory (*e.g.*, flows with massive separation and/or wide shock induced rotational regions). Here, for the

computed numerical results, Eq. 16 has been used neglecting the field term. This has been shown to be legitimate for attached high Reynolds number flows (see [4]), and is also presumably legitimate in the presence of weak shocks (all the cases here analyzed are within this category). However, this work has to be considered the first step toward the analysis of flows with wide rotational regions, where all terms in Eq. 16 are important.

The above formulation may be extended to compressible flows [3,12]. Hence, for viscous transonic flow analysis, once the full-potential distribution has been determined, it can be used both to determine the vorticity beyond the shock and as an input for the boundary layer equations examined in the next Section. Next, the corrective terms in the potential integral representation can be evaluated (Eq. 16), and an iterative procedure can be applied until convergence, in order to obtain the flow field solution.

4. INTEGRAL BOUNDARY LAYER FORMULATION

In this Section we present a brief outline of the methodology we have used in order to solve the rotational flow in the boundary layer. As mentioned above, the rotational region is divided into three regions: the laminar boundary layer, the turbulent boundary layer, and the wake. The laminar boundary layer region has been studied by a modification of the Thwaites method [9], consisting of a compressibility correction to the well-known Thwaites integral, based on the Stewartson transformation (see [14] for details). Next, once detected the transition zone by Michel's method [15], the lag-entrainment method [10] has been applied both in the turbulent region and in the wake. It consists of three differential equations: the first is the classical von Kármán equation, the second is the equation taking into account the flow entering the boundary-layer, whereas the third is derived from the turbulent kinetic energy equation. Furthermore, semi-empirical algebraic closure relationships complete the method. For steady-state flows, the lag-entrainment method is based on the following set of ordinary differential equations

$$\frac{\mathrm{d}\vartheta}{\mathrm{d}x} = \frac{C_f}{2} - (H + 2 - M^2)\frac{\vartheta}{u_e}\frac{\mathrm{d}u_e}{\mathrm{d}x} \tag{17}$$

$$\frac{\mathrm{d}\tilde{H}}{\mathrm{d}x} = \frac{1}{\vartheta}\frac{\mathrm{d}\tilde{H}}{\mathrm{d}H_1}\left[C_E - H_1\left(\frac{C_f}{2} - (H+1)\frac{\vartheta}{u_e}\frac{\mathrm{d}u_e}{\mathrm{d}x}\right)\right] \tag{18}$$

$$\frac{\mathrm{d}\tilde{H}}{\mathrm{d}x} = \frac{1}{\vartheta}(f_1 + f_2) \tag{19}$$

where M is the flow Mach number at the outer edge of the boundary layer. The other terms used to describe the boundary-layer evolution are the displacement thickness δ^*, the momentum thickness ϑ, the entrainment coefficient C_E, the friction coefficient C_f, shape factors $H, \tilde{H}, H_1$, whereas f_1, f_2 are functions of u_e and of some of the integral quantities introduced (for the closure relationships to be used and for detailed information on the method, see [10]).

For attached flows, given u_e and the closure relationships, Eqs. (17)-(19) can be integrated to obtain the turbulent boundary layer solution (direct method). On the other hand, for separated flows the set of differential equations (17)-(19) turns out to be singular (see [4] and [16]) and then the

inverse solution method is nedeed. It consist of (i) adding a fourth differential equation to the set of Eqs. (17)-(19), *e.g.*, that from the definition of the shape factor H, *i.e.*,

$$\frac{\mathrm{d}\delta^*}{\mathrm{d}x} = \vartheta \frac{\mathrm{d}H}{\mathrm{d}x} + H \frac{\mathrm{d}\vartheta}{\mathrm{d}x} \tag{20}$$

(ii) assuming known an integral variable (*e.g.*, δ^*), and (iii) computing the resulting boundary-layer edge velocity. Using an iterative technique, the solution is obtained when the velocity from the boundary layer solution is equal to that given by the external solution.

5. NUMERICAL RESULTS

Some results obtained from the formulation described above will be presented in this Section. First, results concerning 2-D and 3-D transonic configurations (both a fixed wing and a hovering rotor) will be shown in order to demonstrate the capability of the full-potential formulation to predict irrotational flow solutions. Then, the accuracy of the interactive boundary-layer technique will be tested by considering a 2-D subsonic viscous flow configuration results. Finally, results concerning 2-D transonic viscous flow configurations will be presented, in order to validate the full-potential-boundary-layer matching technique. For the numerical results, a zero-th order boundary element discretization has been used, with the addition of field volume elements to take the non-linear terms into account.

Full-potential results

First, we consider a cylinder section with $M_\infty = 0.5$. In Fig. 1 two different mesh size results are compared with a finite volume full-potential solution [17]. The discontinuity predicted by our method appears as an actual jump (confined within one single element); the agreement with the finite volume solution is very good in terms of both shock position and intensity. Note that the convergence of the solution to the steday state is extremely fast and monotone (see Fig. 2).

Results for a rectangular biconvex-section wing with aspect ratio 4, tickness 6%, and angle of attack $\alpha = 1.5°$ are considered in Fig.3: in particular, the comparison with a finite difference solution [18] at the root section reveals a very good agreement. Next, we consider a non-lifting UH-1H hovering rotor, with $M_{TIP} = 0.88$. Figure 4 depicts the pressure coefficient distribution at the radial section $r/R = 0.95$: our preliminary results are compared with both full-potential and Euler results obtained by Prieur, Costes and Baeder [19]. In this case, the agreement between the two full-potential results is not so good, and this maight be due to the coarse grid we have used for the calculations (the shock position reveals a lack of conservativity in our results). However, our solution behaviour is comparable with that obtained in [19].

Viscous subsonic flow results

Then, for the sake of the validation of the internal-external flow interaction technique, we present some results concerning a RAE 2822 airfoil with $M_\infty = 0.6$ and $Re = 3.5 \times 10^6$. Observe that, in this case, the flow remains subsonic all over the airfoil, but the non-linear terms have been included in the computation in order to capture the compressibility effects accurately. In Figs. 5, 6, and 7, computed values of momentum thickness, friction coefficient, and pressure coefficient are compared with experimental data given in [20]. In particular, measured values of boundary layer quantities

obtained at different wake sections, available in [20], are shown ('Experimental 1' and 'Experimental 2', in both Figs. 5 and 6). It is apparent that the agreement is quite good, demonstrating the capability of the interactive boundary-layer technique to capture the viscous effects.

Viscous transonic flow results

Here, we present some preliminary results concerning viscous transonic flow configuration. First, we consider a non-lifting biconvex airfoil with thickness 6%, $M_\infty = 0.858$, and $Re = 2 \times 10^6$. Figure 8 depicts the comparison of the experimental data [21] with both our full-potential results and our interactive boundary-layer results. Starting from the full-potential solution, our viscous solution gets closer to the experimental data, although the agreement is not yet satisfactory. Similar considerations may be made for Fig. 9, where our results are compared with measured data and full Navier-Stokes solution from [22], for a non-lifting NACA 64A010 airfoil, with $M_\infty = 0.8$, and $Re = 2\times10^6$. Finally, we consider a lifting NACA 0012 airfoil, with $M_\infty = 0.775$, $Re = 3.5\times10^6$, and $\alpha = 1°$. Figure 10 shows the measured pressure coefficient distribution [23], the pressure coefficient computed by the full-potential solution, and that computed by the interactive boundary-layer technique. In this case, our viscous results show a bad agreement with the experimental ones in terms of the sharpness of the shock, but this may be due to the poor accuracy of the starting full-potential solution. In fact, it must be pointed out that we have used a nearly converged full-potential solution, since some difficulties in the iterative procedure have been encountered.

6. CONCLUDING REMARKS

A boundary integral equations methodology for the analysis of irrotational and rotational transonic flows has been discussed. Numerical results concerning two- and three-dimensional configurations have also been presented, and compared with experimental data and existing CFD results.

Full-potential results have shown a good level of accuracy when compared with assessed CFD results, even though some lack of conservativity has been observed in the hovering rotor case, where a finer grid analysis is nedeed.

Subsonic viscous flow results have demonstrated the capability of the used interactive technique to capture viscous effects.

For the transonic viscous flow cases encouraging preliminary numerical results have been obtained, even if a better analysis in the shock region (where flow separation may occur) has to be performed.

The extension of the methodology to strong shock and separated flow cases is the next goal of our activity in this field.

ACKNOWLEDGEMENTS

This work was partially supported through a contract from Agusta S.p.A. to the Terza Università di Roma, and through postdoctoral fellowships to Drs. Gennaretti and Iemma.

REFERENCES

[1] Le Balleur, J.C., 'Numerical Viscous-Inviscid Interaction in Steady and Unsteady Flows,' in: Cebeci, T. (Ed.), *Numerical and Physical Aspects of Aerodynamic Flows II*, Springer Verlag, 1984.

[2] Melnik, R.E., 'Turbulent Interactions on Airfoils at Transonic Speeds-Recent Developments,' AGARD CP-291, 1980.

[3] Morino, L., 'Helmholtz and Poincaré Vorticity-Potential Decompositions for the Analysis of Unsteady Compressible Viscous Flows' in: Banerjee P.K. and Morino L. (Eds.), *Developments in Boundary Element Methods, Vol. 6*, Elsevier, Barking, UK, pp. 1-54, 1990.

[4] Gennaretti, M., Una Formulazione Integrale di Contorno per la Trattazione Unificata di Flussi Aeronautici Viscosi e Potenziali, Doctoral Thesis, University of Rome "La Sapienza", Rome, Italy, 1993. (in Italian)

[5] Morino, L., Gennaretti, M., and Shen, S. F., 'Lighthill Transpiration Velocity Revisited: an Exact Formulation,' Meccanica, in print.

[6] Lighthill, M.J., 'On Displacement Thickness', J. Fluid Mech., vol. 4, pp. 383-392, 1958.

[7] Morino, L., and Iemma, U., 'Boundary Integral Equations and Conservative Dissipation Schemes for Full Potential Transonic Flows,' Computational Mechanics, vol. 13, pp. 90-99, 1993.

[8] Iemma, U., Gennaretti, M., and Morino, L., 'Boundary Element Method for Unified Transonic Aerodynamic and Aeroacoustic Analyses of Rotors,' Proceedings of XIX ERF, Cernobbio, Italy, 1993.

[9] Thwaites, B., 'Approximate Calculation of the Laminar Boundary Layer,' Aeronaut. Quart., vol. 1, pp. 245-280, 1949.

[10] Green, J.E., Weeks, D.J., and Brooman, W.F.,'Prediction of turbulent boundary layers and wakes in compressible flow by a lag-entrainment method,' A.R.C.R. & M., no. 3791, 1973.

[11] Iemma, U., and Morino, L., 'Transonic Analysis Using a Boundary Element Method,' Proceedings of XIX ICAS Congress, Anaheim, California, 1994.

[12] Morino, L., 'Boundary Integral Equations in Aerodynamics, Appl. Mech. Rev., vol. 46, no. 8, pp. 445-466, 1993

[13] Iemma, U., Metodi Integrali in Aerodinamica Transonica, Doctoral Thesis, University of Rome "La Sapienza", Rome, Italy, 1994. (in Italian)

[14] Schlichting, H., Boundary-Layer theory, Mc-Grow Hill, 1979.

[15] Michel, R., 'Etude de la transition sur les profils d'aile - establissment d'un point de transition et calcul de la trainée de profil en incompressible', ONERA Report No. 1/1578A, 1952.

[16] Le Balleur, J.C., 'Couplage Visqueux - Non Visqueux: Analyse du Problème Incluant Décollements et Ondes de Choc', La Recherche Aérospatiale, vol. 6, pp. 349-358, 1977.

[17] Salas, M.D., 'Recent Developments in Transonic Euler Flow Over a Circular Cylinder,' NASA TM-83282, 1982.

[18] Steger, J.L., and Caradonna, F.X., 'A Conservative Finite Difference Algorithm for the Unsteady Transonic Full Potential Equation,' NASA TM-81211, 1980.

[19] Prieur, J., Costes, M., and Baeder, J.D., 'Aerodynamic and Acoustic Calculations of Transonic Nonlifting Hovering Rotors,' International Specialists Meeting on Rotorcraft and Rotor Fluid Dynamics, Philadelphia, Pennsylvania, 1991.

[20] Experimental Data Base for Computer Program Assessment, AGARD AR-138, 1979.

[21] Knechtel, E.,D., 'Experimental Investigation at Transonic Speeds of Pressure Distributions over Wedge and Circular Arc Airfoil Sections and Evaluation of Perforated Wall Interference', NASA TND-15, 1959.

[22] Johnson, D.,A., Bachalo, W.,D., 'Transonic Flow about a Two-Dimensional Airfoil: Inviscid and Turbulent Flow Properties', AIAA Paper 78-1117, 1978.

[23] Gregory, N., Wilby, P.,G., 'NPL 9615 and NACA 0012 - A comparison of Aerodynamic Data ', ARC CP 1261, 1973.

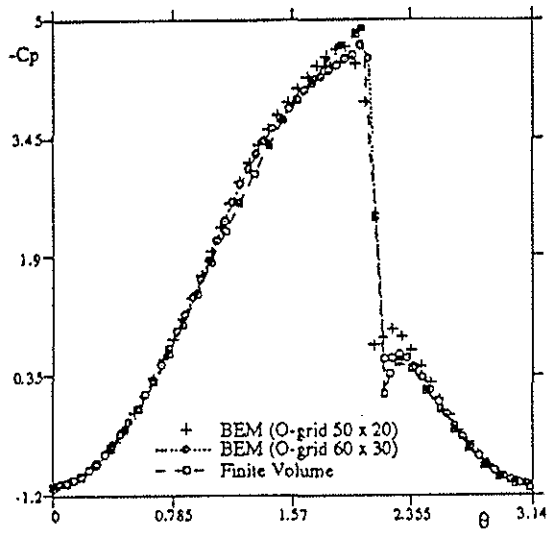

Figure 1. Cylinder at $M_\infty = 0.5$. Pressure coefficient.

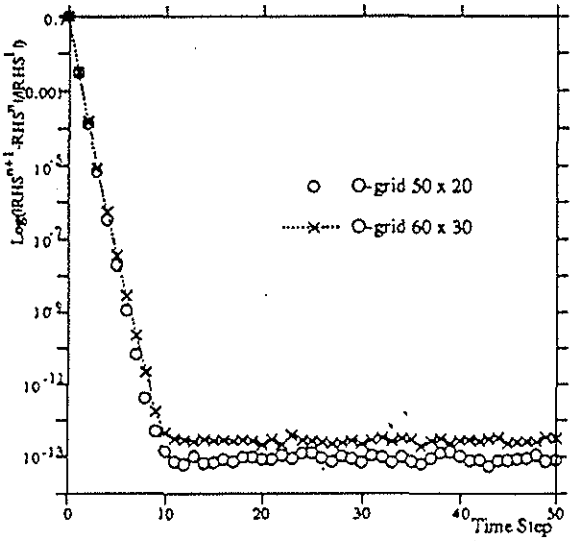

Figure 2. Cylinder at $M_\infty = 0.5$. Convergence history.

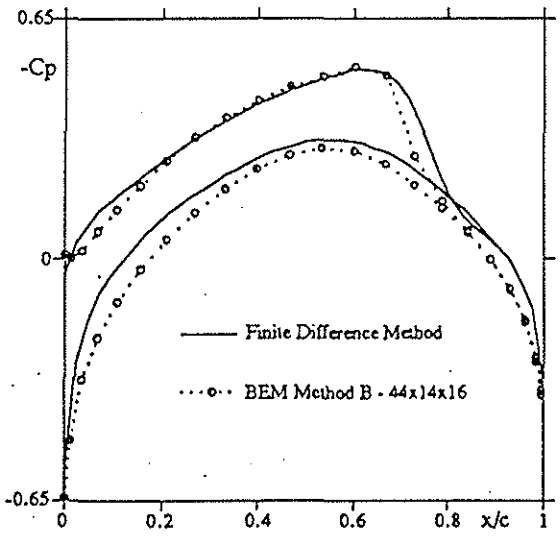

Figure 3. Rectangular wing, $AR = 4$, biconvex 6%, $M_\infty = 0.857$, $\alpha = 1.5°$. Pressure coefficient at the root section.

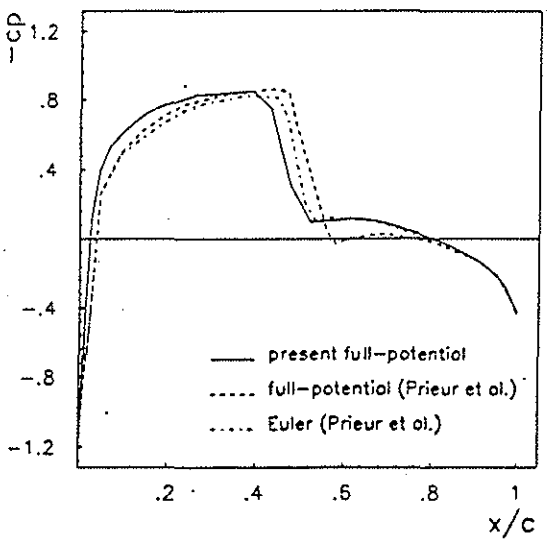

Figure 4. UH-1H rotor, $M_{TIP} = 0.88$. Pressure coefficient at section at $r/R = 0.95$.

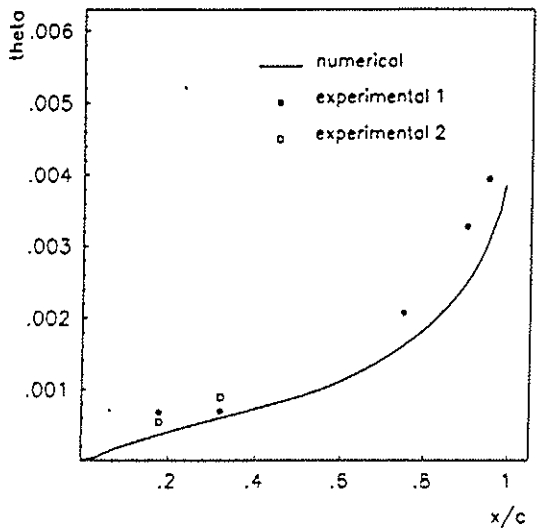

Figure 5. Momentum thickness for RAE 2822 airfoil, $M_\infty = 0.6$, $Re = 6.3 \times 10^6$, $\alpha = 2.57°$.

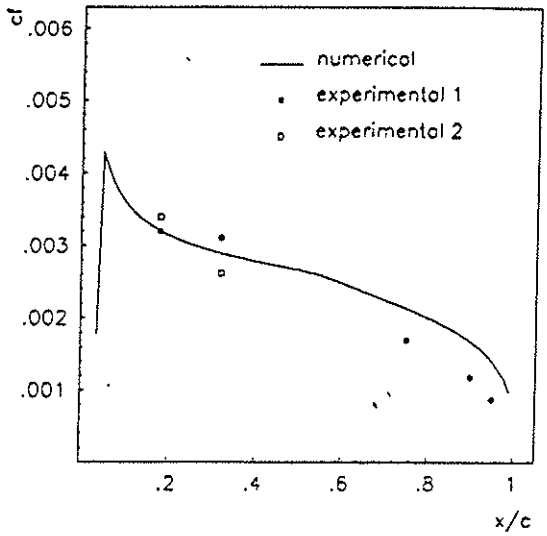

Figure 6. Friction coefficient for RAE 2822 airfoil, $M_\infty = 0.6$, $Re = 6.3 \times 10^6$, $\alpha = 2.57°$.

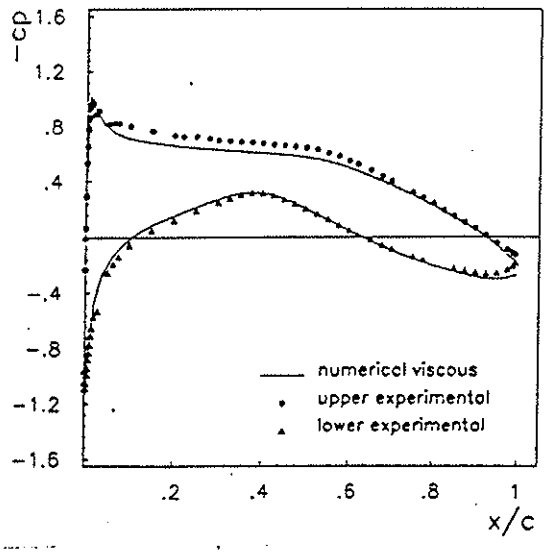

Figure 7. Pressure coefficient for RAE 2822 airfoil, $M_\infty = 0.6$, $Re = 6.3 \times 10^6$, $\alpha = 2.57°$.

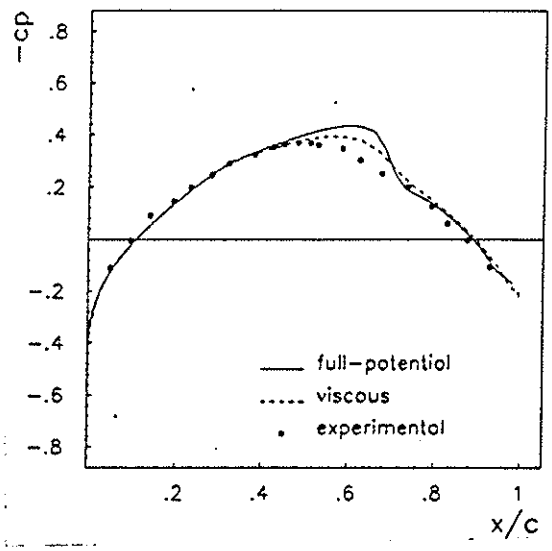

Figure 8. Pressure coefficient for 6% biconvex airfoil, $M_\infty = 0.858$, $\alpha = 0.0°$, $Re = 2 \times 10^6$.

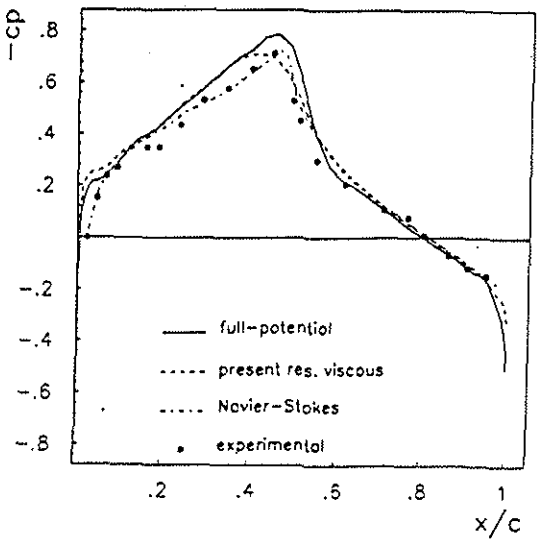

Figure 9. Pressure coefficient for NACA 64A010 airfoil, $M_\infty = 0.8$, $\alpha = 0.0°$, $Re = 2 \times 10^6$.

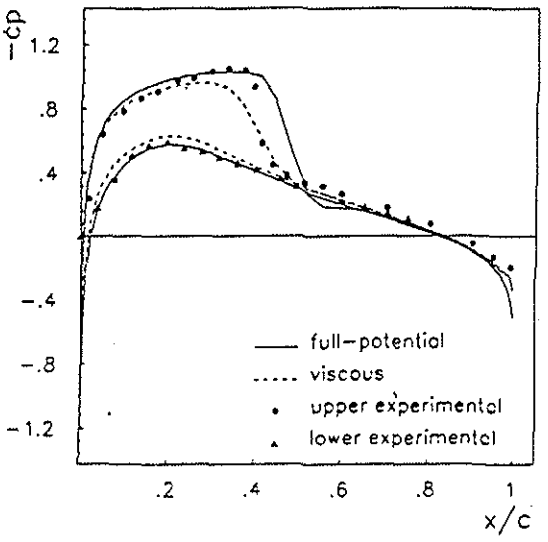

Figure 8. Pressure coefficient for NACA 0012 airfoil, $M_\infty = 0.775$, $\alpha = 1.0°$, $Re = 3.5 \times 10^6$.